Journal of Magnetic Resonance **146,** 140–156 (2000)
doi:10.1006/jmre.2000.2119, available online at http://www.idealibrary.com on IDEAL®

Sideband Patterns from Rotor-Encoded Longitudinal Magnetization in MAS Recoupling Experiments

Susan M. De Paul, Kay Saalwächter, Robert Graf, and Hans W. Spiess[1]

Max-Planck-Institut für Polymerforschung, Postfach 3148, D-55021 Mainz, Germany

Received February 7, 2000; revised April 5, 2000

Recent multiple-quantum MAS NMR experiments have shown that a change in the rotor phase (and, hence, in the Hamiltonian) between the excitation and reconversion periods can lead to informative spinning-sideband patterns. However, such "rotor encoding" is not limited to multiple-quantum experiments. Here it is shown that longitudinal magnetization can also be rotor-encoded. Both homonuclear and heteronuclear *r*otor *e*ncoding of *l*ongitudinal *m*agnetization (RELM) experiments are performed on dipolar-coupled spin-1/2 systems, and the corresponding sideband patterns in the indirect dimension are analyzed. In both cases, only even-order sidebands are produced, and their intensity distribution depends on the durations of the recoupling periods. In heteronuclear experiments using REDOR-type recoupling, purely dipolar sideband patterns that are entirely free of effects due to the chemical-shielding anisotropy can be generated. Advantages and disadvantages of the heteronuclear RELM experiment are discussed in the context of other methods used to measure heteronuclear dipolar couplings.

Key Words: **recoupling; spinning-sideband patterns; magic-angle spinning; *r*otational-*e*cho *do*uble *r*esonance (REDOR); heteronuclear dipolar coupling; longitudinal magnetization.**

INTRODUCTION

Magic-angle spinning (MAS) (*1*) is a well-established technique for improving the sensitivity and resolution of solid-state nuclear magnetic resonance (NMR) spectra. In cases where the spinning frequency exceeds the magnitudes of the anisotropic internuclear interactions, narrow spectral lines can often be obtained. However, it is frequently useful to acquire spectra in the so-called "slow-spinning" regime, where the MAS frequency is less than the static powder linewidth. If the lineshapes are dominated by inhomogeneous interactions (e.g., the chemical-shielding or the heteronuclear dipolar interaction), slow magic-angle spinning will split the spectrum into a pattern of narrow spinning sidebands spaced by integer multiples of the rotation frequency (*2*). The relative intensities of these sidebands contain information about the nature of the dominant anisotropic interactions, and the envelope of the sideband pattern at slow speeds generally resembles the shape of the static powder spectrum (*3, 4*).

In recent years, unusual sideband patterns have been observed in the indirect dimension of multiple-quantum (MQ) MAS experiments on both dipolar-coupled spin-1/2 (*5–11*) and quadrupolar (*9, 12–14*) systems; the patterns were particularly striking in cases where the evolution of total spin coherences was monitored. A total spin coherence is defined as an N-quantum coherence either in an isolated cluster of N dipolar-coupled spins or in an isolated quadrupolar nucleus with a spin-quantum number of $N/2$. For an isolated pair of dipolar-coupled spin-1/2 nuclei, it was found that certain multiple-quantum excitation sequences could generate double-quantum patterns with sidebands appearing only at odd-integer multiples of the spinning frequency (*7, 10*). Patterns with only even-order sidebands could be obtained for triple-quantum spectra of isolated clusters of three dipolar-coupled spins (*8*) as well as for N-quantum spectra of spin-$N/2$ ($N = 3, 5$) nuclei with $\eta^{Q} = 0$ and a negligible second-order quadrupolar interaction (*9*). In cases where such total spin coherences were not excited or where appreciable amounts of undesired interactions (i.e., chemical-shielding anisotropy) were present, both even- and odd-order sidebands were generated, but the patterns still differed significantly from the corresponding single-quantum MAS spectra. Unusual sideband patterns were also observed in the indirect dimension of MQMAS spectra of quadrupolar nuclei with significant second-order quadrupolar perturbations (*12–14*).

A general feature of such multiple-quantum sideband patterns is that the width of the sideband pattern could be made to significantly exceed the strength of the relevant internal Hamiltonian (*5, 6, 12, 13*). Yet, despite their unusual form, the patterns were found to depend in a predictable way upon the strength of the dipolar or quadrupolar coupling and the durations of the excitation and reconversion periods, and thus valuable information could be extracted from them.

The generation of these MQ sideband patterns has been found to be due to several effects (*6, 7, 9, 10, 12–14*): (1) "rotor encoding" of the dipolar or first-order quadrupolar interaction (plus residual chemical-shielding terms in some cases) due to the change in rotor phase (and, hence, in the Hamiltonian) between the multiple-quantum excitation and

[1] To whom correspondence should be addressed. Fax: +49-6131-379320. E-mail: spiess@mpip-mainz.mpg.de.

1090-7807/00 $35.00

reconversion periods; (2) rotor modulation of non-total MQ coherences due to dipolar or quadrupolar evolution during the t_1 period; and (3) rotor modulation of all MQ coherences due to evolution under the chemical-shielding anisotropy (CSA) interaction during the t_1 period. However, there is nothing inherently multiple-quantum about any of these processes. The latter two are simply manifestations of the conventional sideband-generating mechanism in MAS spectra, that is, evolution under an internal Hamiltonian made periodic by sample rotation (*2*). The rotor-encoding phenomenon arises from the rotor-phase dependence of the average Hamiltonians of certain pulse sequences used for "excitation" and "reconversion" (*6, 7, 10, 12, 14*). It is a purely spatial mechanism and does not require concomitant spin evolution during t_1 (*6, 9, 12*). For pulse sequences in which it is present, it often provides the dominant contribution to the sideband intensities observed in the ω_1 dimension.

Phenomena related to rotor encoding in powdered samples have been known for many years. For instance, early attempts to combine chemical-shift exchange spectroscopy with slow MAS led to spurious sidebands in two dimensions when the phase of the rotor at the end of the mixing time was not the same as the phase at either the start or the end of the t_1 period (*15–17*). Clearly, these extra sidebands are manifestations of a type of spectral "encoding" of the change in rotor phase. However, we restrict ourselves here to the definition of rotor encoding relevant to the multiple-quantum experiments discussed above: namely, that the Hamiltonians for both the "excitation" and the "reconversion" periods must depend explicitly upon the rotor phase. In this case, rotor-encoded sidebands will appear only in the ω_1 dimension of the two-dimensional spectrum, and the information that is encoded in these sideband patterns will be determined primarily by the Hamiltonians of the "excitation" and "reconversion" periods.

As mentioned above, rotor encoding is not limited to multiple-quantum coherences. Previous papers (*6, 7*) have already shown that, in theory, longitudinal magnetization should also be rotor-encoded by the pulse sequences used to excite double-quantum coherences, but, to our knowledge, this has never been experimentally demonstrated. The phase cycles of double-quantum experiments were always designed to cancel out contributions from longitudinal magnetization during t_1. Recently, a multiple-quantum-like pulse sequence was used to monitor the decrease in the amount of longitudinal magnetization as a function of the duration of the multiple-quantum excitation and reconversion periods (*18*). However, this filter experiment was carried out under static conditions to measure residual couplings in elastomers and, by definition, does not involve rotor encoding.

One reason for recording spectra of rotor-encoded longitudinal magnetization is that it allows the selective examination of the rotor-encoding process *independent* of the effects of true t_1 evolution. It is well known that internal NMR Hamiltonians do not cause longitudinal magnetization to precess in the rotating frame whereas dipolar, quadrupolar, and chemical-shielding interactions can all affect the precession frequencies of multiple-quantum coherences. In fact, the effects of dipolar couplings and chemical shielding are magnified by the multiple-quantum order (*19*). Nonetheless, if total spin coherences can be excited in an isolated dipolar cluster or in an isolated quadrupolar nucleus, these coherences will not evolve under the dipolar or first-order quadrupolar interaction, respectively (*7, 9, 12*). Furthermore, if the chemical-shielding and second-order quadrupolar anisotropies are also small, the rotor-encoding process will be the dominant factor determining the form of the sideband pattern. However, in the case of rotor-encoded longitudinal magnetization, one does not need to worry about the extent to which the above approximations are justified; rotor encoding is the *only* possible mechanism for sideband generation in ω_1. Thus, sideband patterns from rotor-encoded longitudinal magnetization should augment the other techniques in yielding particularly clear-cut dipolar patterns.

In this paper we examine the sideband patterns generated by rotor encoding of longitudinal magnetization for both homonuclear and heteronuclear dipolar-coupled spin-1/2 systems. We demonstrate that it is possible to generate sideband patterns that depend only on the heteronuclear dipolar coupling and the durations of the encoding periods. Finally, we discuss this technique in the context of other NMR methods for distance measurement in solids.

THEORY

In this section, the basic ideas behind *r*otor *e*ncoding of *l*ongitudinal *m*agnetization (RELM) will be outlined in a general way. Subsequently, actual pulse sequences that can be used for heteronuclear and homonuclear RELM will be examined in more detail.

Principles of RELM

A schematic of the basic pulse sequence used for RELM is given in Fig. 1. The pulse sequence consists of several stages. The first stage is a preparation period during which the system is placed in a desirable initial state. For the heteronuclear RELM experiment discussed below (see Fig. 2), this usually consists of a cross-polarization step followed by a flip-back pulse on the S channel to create S_z magnetization. For the homonuclear RELM experiment presented in this paper (see Fig. 3), there is no preparation period at all, and the equilibrium state of the system is the starting point. The next stage of the experiment is the first "encoding" period, τ_{enc1}, during which the spin system evolves under an internal NMR Hamiltonian. In order for the rotor-encoding mechanism to function, the amplitude of the average Hamiltonian for the encoding period must depend on the Euler angle, γ, describing the phase of the internuclear vector with respect to the rotor phase. The simplest such encoding sequence consists of two 90° pulses with a short period of free dipolar evolution between them (*6, 10*). However, such a sequence can only generate sidebands when

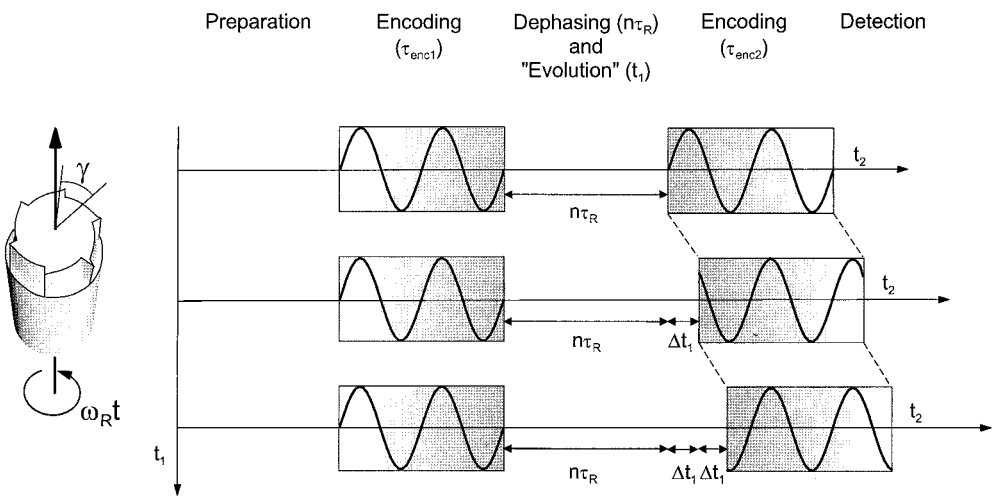

FIG. 1. Schematic illustration of the principle of rotor encoding in the RELM experiment. The two encoding periods must have average Hamiltonians which depend explicitly on the rotor phase. In the simplest case, these two average Hamiltonians are identical. The encoding periods are separated by both a rotor-synchronized dephasing and a non-rotor-synchronized evolution (t_1) period. When t_1 equals zero, the two encoding sequences have the same initial rotor phase. As t_1 is incremented, the rotor-phase dependence of the second encoding period changes relative to that of the first encoding period. This leads to an amplitude modulation of the signal in the t_1 dimension even if no coherences evolve during this time.

the dipolar coupling is significantly larger than the spinning frequency. In the general case, a recoupling sequence must be applied. Laboratory-frame recoupling sequences such as *r*otational-*e*cho *do*uble-*r*esonance (REDOR) (*20*), *d*ipolar *r*ecovery *a*t the *m*agic *a*ngle (DRAMA) (*21*), or *ba*ck to *ba*ck (BABA) (*22*) have the proper γ dependence for RELM, but rotating-frame sequences such as C7 (*23*) and its derivatives do not.

Up to this point, the pulse sequence strongly resembles previous pulse sequences for multiple-quantum spectroscopy of dipolar-coupled spins, with the first encoding period corresponding to the "excitation" period in a multiple-quantum experiment. However, longitudinal magnetization is also generated by the recoupling sequences applied during τ_{enc1} (see below). In a typical multiple-quantum experiment this longitudinal magnetization is phase-cycled away, but by using a different phase cycle, it is possible to cycle away the multiple-quantum magnetization instead.

True zero-quantum coherences (between two or more spins) cannot be separated from longitudinal magnetization by phase cycling (*19*), but such coherences will decay faster (at a rate of $1/T_2^{ZQC}$) than the single-spin longitudinal magnetization terms (at a rate of $1/T_1$). By waiting an integral number of rotor periods, therefore, it should be possible to suppress true zero-quantum coherences while retaining longitudinal magnetization. For an isolated two-spin system, a pulse sequence that will not generate any true zero-quantum coherences can be designed. For more complicated spin systems, however, a pulse sequence that generates zero-quantum coherences is preferable, as will be discussed below.

A non-rotor-synchronized evolution, or t_1, period follows the dephasing period. Since the precession frequency of longitudinal magnetization is not affected by internal NMR Hamiltonians, one cannot properly speak of an "evolution" period in the RELM experiment. However, during the time t_1 the phase of the rotor will change from its initial value (see Fig. 1). Let us now consider an experiment in which the pulse sequence applied during the first encoding period is applied again in a second encoding period, τ_{enc2}, after the time t_1. (This second encoding period is analogous to the "reconversion" period in a multiple-quantum spectrum.) The Hamiltonian for the second encoding period will differ from the Hamiltonian for the first encoding period if the rotor phase has changed, and both Hamiltonians will affect the signal that is eventually detected. A series of FIDs which are amplitude-modulated as a function of the change in rotor phase or, in other words, as a function of t_1 is, therefore, obtained. Fourier transformation of this amplitude-modulated signal leads to a sideband pattern in ω_1.

The rotor-encoding mechanism described above is, of course, also present in the multiple-quantum experiments described previously. However, since no evolution occurs during the t_1 period in RELM, the RELM sideband patterns are influenced only by the Hamiltonians of the two encoding periods. Thus, if the recoupling Hamiltonian is purely dipolar and free of chemical-shielding effects (as is the case in the heteronuclear sequence described below), the resulting RELM sideband patterns will also be purely dipolar. In contrast, double-quantum coherences are affected during t_1 by both chemical-shielding evolution and couplings to remote spins. The sidebands generated in a double-quantum experiment will, therefore, depend on several parameters, and interpretation of their intensities can be more ambiguous than in the RELM case.

Heteronuclear RELM Using REDOR-Type Recoupling Sequences

Figure 2 shows the pulse sequence used for the heteronuclear RELM experiments described in this paper. During the

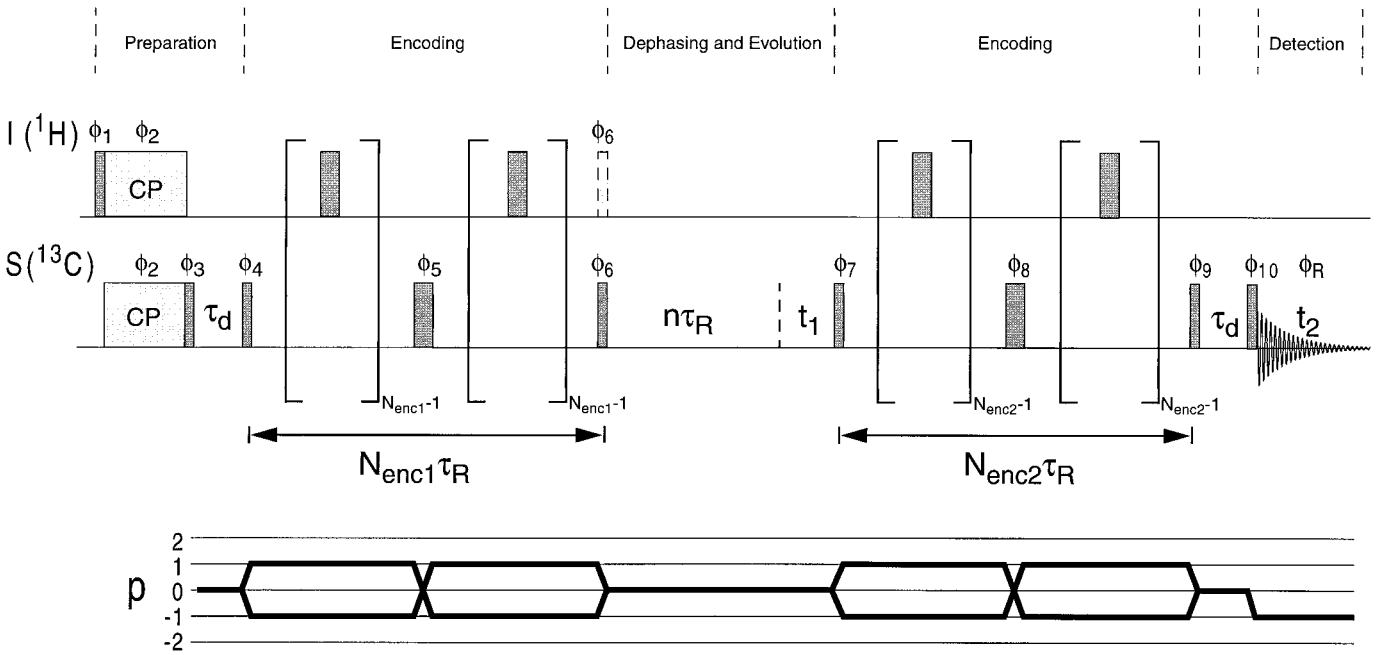

FIG. 2. Pulse sequence for a heteronuclear RELM experiment involving REDOR-type recoupling. A cross-polarization step is typically used to provide sufficient *S*-spin polarization (S_z) for the start of the experiment. Each encoding period consists of a REDOR-type recoupling train of 180° pulses bracketed by 90° pulses on the carbons. For systems with more than one *I* spin, an extra 90° pulse on the *I* spins is required (as described in the text). A dephasing period with a duration equal to an integral number of rotor periods follows the first encoding period, and the t_1 period follows the dephasing period. Another dephasing period (which need not be rotor-synchronized) follows the second encoding period, and the signal is detected after a 90° read pulse. *XY*-4 phase cycling (*64*) is used for the 180° pulse train on the *I* channel. The coherence transfer pathway for the *S* spins is depicted below the pulse sequence, and the phases of the pulses are given in Table 1.

preparation period, *S*-spin longitudinal magnetization is generated by cross polarization from the protons followed by a flip-back pulse on the *S* channel.

Encoding of the heteronuclear dipolar interaction is achieved by using a REDOR (*20, 24*) pulse train as the recoupling sequence (*11, 25–27*). First, a 90° pulse is used to generate S_x magnetization. Then the REDOR pulses are applied for N_{enc1} rotor periods. At the end of this time, the magnetization will have evolved according to

$$S_x\cos(N_{\text{enc1}}\Phi_{IS}(0)) + 2S_yI_z\sin(N_{\text{enc1}}\Phi_{IS}(0)), \qquad [1]$$

where Φ_{IS} has the form

$$\Phi_{IS}(t) = \frac{D_{IS}}{\omega_{\text{R}}}\,2\sqrt{2}\,\sin 2\beta_{IS}\sin(\omega_{\text{R}}t + \gamma_{IS}), \qquad [2]$$

as determined by average-Hamiltonian theory for a two-spin system using the secular approximation. Here, ω_{R} is the MAS frequency, and β_{IS} and γ_{IS} are Euler angles representing the orientation of the dipolar vector with respect to the rotor reference frame. D_{IS} is the dipolar coupling constant (in units of angular frequency)

$$D_{ij} = \left(\frac{\mu_0}{4\pi}\right)\hbar\,\frac{\gamma_i\gamma_j}{r_{ij}^3}, \qquad [3]$$

where r_{ij} is the internuclear distance. Note that at the end of a REDOR-type recoupling train, all chemical-shielding anisotropy and offset effects have been removed, and only a net heteronuclear dipolar evolution remains.

In a heteronuclear double-quantum experiment (*10, 11*), the second term in Eq. [1] would be converted into double (and zero)-quantum magnetization by a 90° pulse applied to the *I* spins, and the first term in Eq. [1] would be cycled away. However, in the RELM experiment, it is the first term in Eq. [1] that is retained and the second one that is suppressed. Thus, a 90° pulse about the $+y$ or $-y$ axis is applied to the *S* spins to convert the S_x term into longitudinal (S_z) magnetization (with alternate storage along the $+z$ and $-z$ axes to suppress axial peaks). For the case of an isolated *I*–*S* spin pair, no 90° pulses need be applied to the *I* spins, and the remaining antiphase magnetization (S_yI_z) can simply be allowed to decay during a dephasing time that lasts an integral number of rotor periods. In fact, this dephasing time is not strictly necessary for an isolated two-spin system since antiphase magnetization can be separated from longitudinal magnetization by phase cycling. However, when more than one *I* spin is present, the situation

becomes more complicated, as will be discussed below, and pulses should also be applied to the I spins.

Since no evolution occurs during t_1, we can proceed immediately to calculating the form of the modulation during the second encoding period. Again, a 90° pulse converts S_z magnetization into transverse magnetization which evolves under the REDOR-type recoupling Hamiltonian, and only the magnetization proportional to S_x is retained at the end of the encoding period. However, because the rotor has acquired an additional phase, $\omega_R t_1$, the modulation during τ_{enc2} will, in general, be different from that in τ_{enc1}. The signal generated in the indirect dimension of the two-dimensional experiment therefore has the form

$$S(t_1;\, t_2 = 0) \propto \langle \cos(N_{enc1}\Phi_{IS}(0))\cos(N_{enc2}\Phi_{IS}(t_1))\rangle, \quad [4]$$

where the brackets represent a powder average over all possible orientations. By inserting Eq. [2] into Eq. [4] and using the relation (*28*)

$$\cos(x\, \sin(\omega_R t + \gamma_{ij})) = J_0(x) + 2\sum_{k=1}^{\infty} J_{2k}(x)\cos(2k\omega_R t + 2k\gamma_{ij}), \quad [5]$$

one can see that only even-order sidebands (at positions $m \cdot \omega_R$ with $m = 0, \pm 2, \pm 4, \ldots$) will be present in the frequency domain. The intensities of these sidebands depend only on the strength of the dipolar coupling, allowing spin-pair distances to be extracted by fitting the sideband patterns. For short recoupling times, only low-order sidebands are observed; higher-order sidebands grow in as the recoupling time is increased. A more detailed examination of the sideband intensities is presented in the Appendix.

For multispin systems the situation becomes slightly more complicated. For instance, evolution under heteronuclear dipolar couplings to two I spins (neglecting I-spin homonuclear coupling) produces the following terms at the end of the first encoding period:

$$\begin{aligned} &S_x\cos(N_{enc1}\Phi_{I^{(1)}S}(0))\cos(N_{enc1}\Phi_{I^{(2)}S}(0)) \\ &\quad + 2S_yI_z^{(1)}\sin(N_{enc1}\Phi_{I^{(1)}S}(0))\cos(N_{enc1}\Phi_{I^{(2)}S}(0)) \\ &\quad + 2S_yI_z^{(2)}\cos(N_{enc1}\Phi_{I^{(1)}S}(0))\sin(N_{enc1}\Phi_{I^{(2)}S}(0)) \\ &\quad - 4S_xI_z^{(1)}I_z^{(2)}\sin(N_{enc1}\Phi_{I^{(1)}S}(0))\sin(N_{enc1}\Phi_{I^{(2)}S}(0)). \end{aligned} \quad [6]$$

A 90° pulse about S_y alone will store not only the first term of Eq. [6] as longitudinal magnetization but also the last term of Eq. [6] as three-spin dipolar order ($S_zI_z^{(1)}I_z^{(2)}$). Although the rotor modulation due to such a term can easily be calculated, sideband analysis is complicated by the fact that the relaxation time of such a multispin term would most likely differ from that of the single-spin term, and thus the weighting of the different contributions would be unequal. Fortunately, simultaneous 90° pulses about I_y and S_y at the end of the first encoding period will convert the $S_xI_z^{(1)}I_z^{(2)}$ term into $S_zI_x^{(1)}I_x^{(2)}$. The latter term is a combination of antiphase double-quantum and antiphase zero-quantum terms, and it should decay (along with the single-quantum antiphase terms) during the rotor-synchronized dephasing period. Then only the first term of Eq. [6] will contribute to the RELM spectrum.

The above treatment can be extended to systems with more than two I spins, and it can easily be shown (*29*) that, as in the REDOR experiment, an extra cosine factor is obtained for each additional S–I coupling (assuming homonuclear couplings can be neglected). In the case of RELM, of course, each S–I coupling also acquires a cosine factor from the second encoding period. Thus, analytical expressions for RELM sideband patterns can be derived even for complicated spin topologies. In general, such expressions will depend not only on internuclear distances but also on the angles between the internuclear vectors.

A particularly simple case is that of a methyl group, where rapid threefold jumps average the positions of the three C–H bonds (*29–31*). Since the effects of homonuclear couplings between the methyl protons can be neglected for REDOR recoupling (*29*), the carbon longitudinal magnetization will acquire three cosine factors (one for each C–H bond) in each encoding period, leading to a signal of the form

$$\begin{aligned} S(t_1;\, t_2 = 0) \propto \langle &\cos(N_{enc1}\Phi_{I^{(1)}S}(0))\cos(N_{enc1}\Phi_{I^{(2)}S}(0)) \\ &\times \cos(N_{enc1}\Phi_{I^{(3)}S}(0))\cos(N_{enc2}\Phi_{I^{(1)}S}(t_1)) \\ &\times \cos(N_{enc2}\Phi_{I^{(2)}S}(t_1)) \\ &\times \cos(N_{enc2}\Phi_{I^{(3)}S}(t_1))\rangle. \end{aligned} \quad [7]$$

For an idealized methyl group (i.e., perfect C_3 rotational symmetry, equivalent C–H bond lengths), the three frequencies are identical ($\Phi_{I^{(1)}S} = \Phi_{I^{(2)}S} = \Phi_{I^{(3)}S}$). Furthermore, the fast jumps about the C_3 axis scale the effective C–H dipolar coupling by $P_2(\cos\theta)$, which equals $-\frac{1}{3}$ for a perfect tetrahedron. Using the trigonometric relation

$$\cos^3\left(\frac{\zeta}{3}\right) = \frac{1}{4}\left(3\cos\left(\frac{\zeta}{3}\right) + \cos(\zeta)\right), \quad [8]$$

where $\zeta/3 = N_{enc}\phi_{IS}P_2(\cos(70.53°))$ and ϕ_{IS} is the dipolar phase for a non-motionally averaged C–H pair, one can see that the dephasing of a methyl group in a REDOR experiment (and, similarly, the methyl group pattern in the dipolar dimension of a separated local field (*32*) or other heteronuclear dipolar correlation experiment) is equivalent to the sum of the dephasing due to one motionally averaged C–H pair (i.e., with one-third of the dipolar interaction of a static C–H pair) and the dephasing due to a static C–H pair, with weighting factors of 0.75 and 0.25, respectively. This weighting has been mentioned previously in the literature (*30, 32*) although it was derived by a different argument (popu-

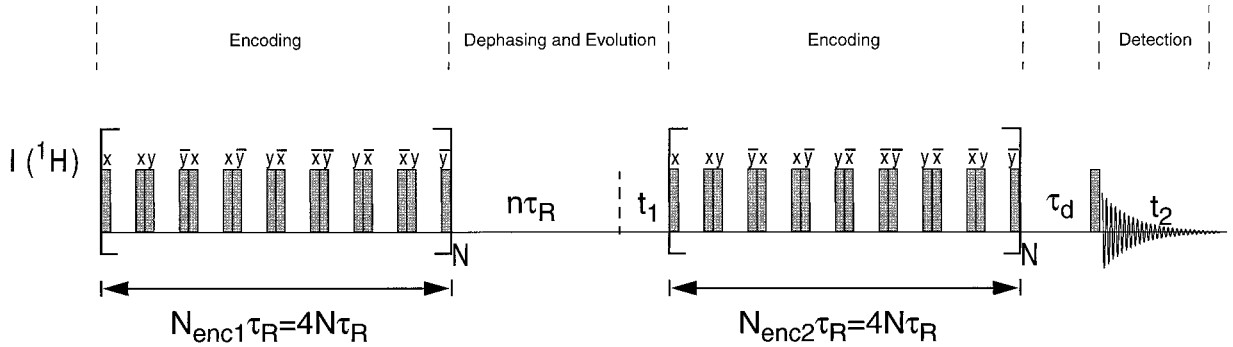

FIG. 3. Pulse sequence for the homonuclear RELM experiment involving BABA recoupling. The offset-compensated, four-rotor cycle version of the BABA experiment (*22*) was used during each encoding period. Phase cycling of the pulses is described in the text.

lations of spin states from perturbation theory). The relative weighting of the sum and difference dipolar tensors thus arises naturally from product-operator theory.

For the methyl group in a RELM experiment, the time-domain signal in the indirect dimension consists of a product of two cosine-cubed terms: one containing $\Phi_{IS}(0)$ and one containing $\Phi_{IS}(t_1)$ (see Eq. [7]). Using Eqs. [7] and [8] one can show that the methyl group RELM signal will consist of 9/16 of a RELM pattern for a C–H pair with one-third of the static coupling plus 1/16 of the RELM pattern for a C–H pair with the full static coupling plus 3/16 each of patterns due to cross terms involving both reduced and full couplings. The pattern for the C–H pair with one-third of the static coupling dominates the appearance of the spectrum since that pattern has the highest net intensity and this intensity is concentrated in the fewest sidebands. RELM sideband patterns for an ideal methyl group can easily be simulated. Treatments of nonidealized methyl groups (i.e., with unequal bond lengths and deviation from perfect tetrahedral symmetry) have been described in the literature (*33*).

Since the centerband in the ω_1 dimension of the RELM experiment can have contributions from spins which relax during the course of the experiment (leading to axial peaks) as well as from *S* spins that are not coupled to *I* spins, its intensity is inherently unreliable. However, since the higher-order sidebands do not suffer from such effects, it is possible to neglect the centerband and fit the relative intensities of the remaining sidebands. This is the approach that is followed in this paper.

Homonuclear RELM Using the Back-to-Back Recoupling Sequence

The RELM method is not limited to heteronuclear interactions; Fig. 3 shows a possible pulse sequence for homonuclear spins, which uses the BABA (*22*) recoupling sequence during the two encoding periods. For an isolated spin pair with negligible chemical-shielding anisotropy, the state of the spin system after the first BABA encoding period is given by

$$T_{1,0}\cos(N_{\text{enc1}}\Phi'_{II}(0)) - 2i(T_{2,2} - T_{2,-2})\sin(N_{\text{enc1}}\Phi'_{II}(0)), \quad [9]$$

where (*22*)

$$\Phi'_{II}(t) = \frac{D_{II}}{\omega_R} 3\sqrt{2}\,\sin 2\beta_{II}\sin(\omega_R t + \gamma_{II}) \quad [10]$$

and the dipolar coupling constant, D_{II}, is defined according to Eq. [3]. Note that the spherical tensor operators in Eq. [9] are defined according to (*34*) $T_{1,0} = I_z^{(1)} + I_z^{(2)}$ and $T_{2,\pm 2} = \frac{1}{2} I_{\pm}^{(1)} I_{\pm}^{(2)}$, where $I_{\pm} = I_x \pm iI_y$. The term $T_{1,0}$ corresponds to longitudinal magnetization while the terms $T_{2,\pm 2}$ represent double-quantum coherences.

As in the heteronuclear RELM experiment, the longitudinal magnetization (see Eq. [9]) at the end of the encoding period is cosine-modulated. The change in rotor phase during t_1 will change the effective modulation frequency during the second encoding period, leading to a signal of the form

$$S(t_1;\, t_2 = 0) \propto \langle \cos(N_{\text{enc1}}\Phi'_{II}(0))\cos(N_{\text{enc2}}\Phi'_{II}(t_1))\rangle. \quad [11]$$

Note that Eq. [11] has the same form as Eq. [4]. By using Eq. [5] one can again show that only even-order sidebands will be generated.

The above derivation (Eqs. [9] and [10]) assumed an isolated spin pair with negligible chemical-shielding anisotropy on both spins. For three or more strongly coupled homonuclear spins (even without any chemical-shielding anisotropy), it is no longer possible to derive analytical formulas for the sideband intensities, except in rare cases of particularly favorable geometries, because the dipolar Hamiltonian will not commute with itself at two different times. Furthermore, the BABA sequence, like all laboratory-frame homonuclear recoupling sequences developed to date, recouples not only the homonuclear dipolar interaction but part of the chemical-shielding anisotropy as well. Thus, the sideband patterns that are obtained will depend on the magnitudes and orientations of the CSA tensors of both spins (as will be demonstrated below). Unfortunately, the homonuclear recoupling sequences that are least sensitive to CSA orientations (such as C7) do not have the appropriate γ dependence for the rotor-encoding mechanism to function.

TABLE 1
Full 64-Step Phase Cycle for the Heteronuclear RELM Experiment (see Fig. 2)

ϕ_1	$\{+x\ -x\}_{32}$
ϕ_2	$\{-y\}_{64}$
ϕ_3	$\{-x\ +x\}_{32}$
ϕ_4	$\{+x\ +x\ +y\ +y\ -x\ -x\ -y\ -y\}_8$
ϕ_5	$\{+y\ +y\ -x\ -x\ -y\ -y\ +x\ +x\}_8$
ϕ_6	$\{-x\ +x\ -y\ +y\ +x\ -x\ +y\ -y\}_8$
ϕ_7	$\{+x\ -x\}_{32}$
ϕ_8	$\{+y\}_{64}$
ϕ_9	$\{-x\ +x\}_{16}\ \{+x\ -x\}_{16}$
ϕ_{10}	$\{-x\ +x\}_4\ \{-y\ +y\}_4\ \{+x\ -x\}_4\ \{+y\ -y\}_4\ \{+x\ -x\}_4\ \{+y\ -y\}_4\ \{-x\ +x\}_4\ \{-y\ +y\}_4$
ϕ_R	$\{+x\}_8\ \{+y\}_8\ \{-x\}_8\ \{-y\}_8\ \{+x\}_8\ \{+y\}_8\ \{-x\}_8\ \{-y\}_8$

Note. The subscripts indicate how many times the phase sequence in braces should be repeated.

For these reasons, the homonuclear RELM experiment presented in this paper (see Fig. 3) is expected to have limited utility for nuclei other than protons (which have small CSA tensors).

EXPERIMENTAL

Experiments were performed on a Bruker DSX spectrometer with a ^{1}H frequency of 300.2 MHz and a ^{13}C frequency of 75.49 MHz and on a Bruker DRX spectrometer with a ^{1}H frequency of 700.1 MHz and a ^{13}C frequency of 176.05 MHz. Commercial Bruker double-resonance 2.5-mm MAS probes, which permit spinning frequencies of up to 35 kHz, were used for all experiments. Typical 90° pulse lengths were 2 μs ($\omega_1/(2\pi) = 125$ kHz) on both channels. In experiments where a cross-polarization step was used, the proton 90° pulse length was 3 μs ($\omega_1/(2\pi) = 83.3$ kHz), and an ascending linear ramp was performed over the first matching sideband on the carbon channel. Contact times were optimized to provide maximum ^{13}C signal intensity. TPPM (*35*) dipolar decoupling with alternating 30° phases and flip angles of approximately 170° (3.8-μs pulses of strength $\omega_1/(2\pi) = 125$ kHz) was used during detection. Typical dephasing delays (τ_d) after the cross-polarization step and before the read out pulse were 10 ms. The rotor-synchronized dephasing delay (after the first encoding period) was in the range of 400 μs to 1 ms. For such relatively short dephasing delays, active rotor synchronization was not necessary although it could easily be implemented by triggering the rotor synchronization before each encoding period (*33*). Recycle delays were 1–3 s for all samples except for the trichloroacetic acid, where a 15-s recycle delay was used. Between 64 and 128 t_1 slices were recorded for each experiment.

The phase cycles for the RELM experiments are indicated in Figs. 2 and 3 and Table 1. In both experiments, the phases of the pulses in the first encoding period are cycled (as a block) relative to those of the second encoding period in steps of 90° to suppress double-quantum coherences during the evolution period. Further cycling of the read pulse in steps of 90° suppresses unwanted coherences present during the second dephasing period. To prevent axial peaks due to T_1 relaxation, the phase of the last 90° pulse in each encoding period is cycled to alternately store the magnetization along $+z$ or $-z$ during the subsequent dephasing period. Full cycling through all possible combinations of $+z$ and $-z$ magnetization (along with the rest of the phase cycling described above) leads to a 64-step phase cycle. In practice, however, it was found that even a partial phase cycling of the $+z$ and $-z$ magnetization (the first 32 steps of the cycle shown in Table 1) gave rise to the same centerband intensities. Since axial peaks only distort the centerband intensity and since it is usually not advisable to include the centerband in fits of RELM spectra, one could also choose to omit the axial-peak-suppression cycling entirely and use a 16-step phase cycle. In all experiments presented in this paper, however, at least a 32-step phase cycle was employed. In the experiments which used cross polarization, spin-temperature alternation was also included (see Table 1), but the phases of the flip-back pulses were correspondingly adjusted so that the total length of the phase cycle was unaffected.

Additional experimental details are given in the figure legends. To process each data set, a complex Fourier transform was performed over the t_2 dimension followed by a cosine (real) Fourier transform over the t_1 dimension, which is purely amplitude-modulated. In fact, it is not possible to use TPPI with longitudinal magnetization since one cannot phase shift a zeroth-order coherence.

To test the performance of the pulse sequences, initial experiments were carried out on a sample of triply ^{13}C-labeled L-alanine (obtained from Isotec, Inc.) mixed with natural-abundance L-alanine (from Aldrich) in a ratio of 1:9. Heteronuclear RELM experiments were also performed on natural-abundance L-tyrosine · HCl, which was prepared by dissolving L-tyrosine (Fluka) in concentrated hydrochloric acid and evaporating. Homonuclear ^{1}H RELM experiments were performed on natural-abundance trichloroacetic acid (Hoechst), which is very hygroscopic. Before measurements were performed on this sample, it was dried under vacuum overnight, and a glove box was used to transfer it to a 2.5-mm rotor. The rotor was not sealed, but the endcaps fit tightly enough to slow the rate of water absorption to an acceptable level, permitting 1 day's worth of experiments to be performed.

To extract an internuclear distance from a spinning-sideband pattern, a nonlinear least-squares fit of the analytical spectrum (the cosine Fourier transform of Eq. [4], [7], or [11]) to the experimental spectrum was performed using the Levenberg–Marquardt algorithm from Numerical Recipes (*36*). The dipolar coupling constant (D_{ij}), a scaling factor for the peak intensities, and the time constant for apodization of the simulated FID were all varied freely to minimize χ^2, but the centerband region was excluded from the fit. The signal-to-noise ratio of the experimental spectrum was used to estimate the standard deviation of the measured data, and the error bars for the

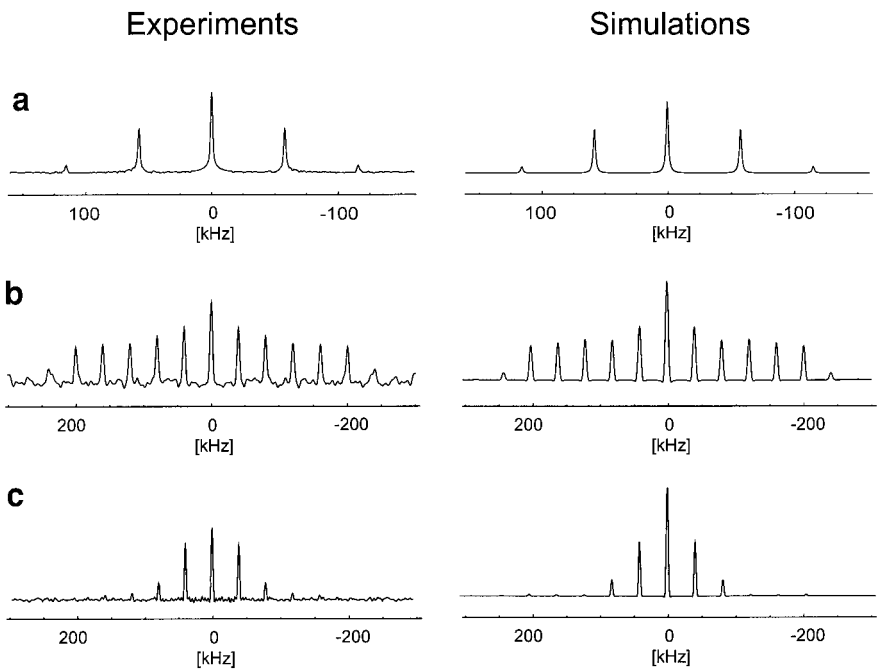

FIG. 4. ^{1}H–^{13}C RELM spectra of L-alanine under various conditions. The experimental spectra (which were recorded on a 300-MHz spectrometer) are on the left side of the figure and the best-fit simulations are on the right side. In all cases the intensity of the centerband was omitted from the fit. (a) The α (methine) carbon with $\omega_R/(2\pi) = 30$ kHz and $N_{enc1} = N_{enc2} = 2$, (b) the α carbon with $\omega_R/(2\pi) = 20$ kHz and $N_{enc1} = N_{enc2} = 4$, and (c) the β (methyl) carbon with $\omega_R/(2\pi) = 20$ kHz and $N_{enc1} = N_{enc2} = 4$.

internuclear distance were determined from the covariance matrix calculated by the algorithm. These error bars do not include the effects of pulse imperfections, etc., which might also be expected to affect the measured sideband intensities.

Density matrix simulations were performed using the GAMMA (*37*) simulation package and carrying out a small-step numerical integration of the Liouville–von Neumann equation. Typical time steps were on the order of 0.5 μs. Powder averaging was performed with 2200 crystallite orientations distributed over the sphere according to the method of Cheng *et al.* (*38*).

Numerical integration of the formula for the sideband intensities (see Appendix) was performed using MATLAB (*39*).

RESULTS AND DISCUSSION

Heteronuclear RELM with $N_{enc1} = N_{enc2}$

To test the pulse sequence of Fig. 2, proton–carbon RELM experiments were performed on a sample of 10% fully labeled L-alanine over a variety of different spinning frequencies and recoupling times. High spinning frequencies ($\geq$20 kHz) were used to lessen the effects of homonuclear couplings among protons (*4, 10*).

Figures 4a and 4b show sideband patterns in ω_1 for the α (methine) carbon of L-alanine under different experimental conditions. For the spectrum in Fig. 4a, the spinning frequency was 30 kHz and $N_{enc1} = N_{enc2} = 2$ while for the spectrum in Fig. 4b, the spinning frequency was 20 kHz and $N_{enc1} = N_{enc2} = 4$. Since the dipolar coupling to the directly bound proton is very strong and is expected to dominate the signal, one can treat the system as an isolated spin pair and fit the sideband pattern to the Fourier transform of Eq. [4]. Note that the dipolar coupling constant, D_{IS}, is the only adjustable NMR parameter. The best-fit spectra are shown on the right-hand side of Fig. 4. The distances extracted from the fits were 1.15 $\pm$ 0.03 Å for the spectrum in Fig. 4a and 1.14 $\pm$ 0.01 Å for the spectrum in Fig. 4b, and consistent values were obtained for spectra recorded at other excitation times and spinning frequencies (data not shown). Figure 4c shows a sideband pattern for the β (methyl) carbon in L-alanine for $\omega_R/(2\pi) = 20$ kHz and $N_{enc1} = N_{enc2} = 4$. This pattern was fit to a simulation based on Eq. [7] and assuming an idealized methyl group. It corresponds to a rigid C–H distance of 1.12 $\pm$ 0.01 Å. As expected from theory, the pattern is dominated by the pattern for a C–H coupling scaled by $\frac{1}{3}$, with low-intensity higher-order peaks (from the stronger effective coupling and the cross terms) also present.

The distances obtained using RELM are slightly longer than the distances determined from neutron diffraction (1.093 Å for the methine carbon, 1.08 Å for the methyl carbon) (*40*). However, solid-state NMR measurements generally give longer distances than neutron diffraction measurements (*41, 42*), and this has been attributed to differences in the ways the two experiments probe vibrational averaging (*43–45*).

Because the modulation in t_1 depends only on the rotor phase, the entire information content of a RELM experiment

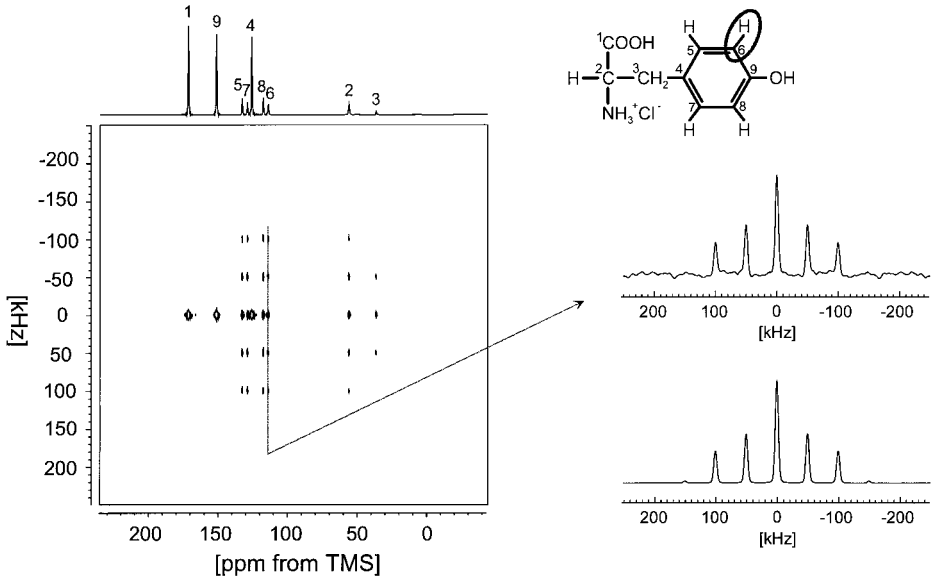

FIG. 5. ^{1}H–^{13}C RELM spectrum of L-tyrosine · HCl for $\omega_R/(2\pi) = 25$ kHz and $N_{enc1} = N_{enc2} = 2$. 128 t_1 slices were acquired with 1024 transients each (total acquisition time: 2 days) on a 300-MHz spectrometer. A two-dimensional contour plot of the RELM experiment is shown along with a skyline projection onto the direct axis; the carbons that are not directly bound to protons undergo the least dephasing and, therefore, have the highest intensity. Both the experimental and the simulated RELM sideband patterns for the C6 carbon (circled in the formula) are also shown. The internuclear distances extracted from this spectrum are listed in Table 2.

can be obtained from a single rotor period of t_1 evolution. Furthermore, since $T_1 \gg \tau_R$, the signal will hardly decay during this time. This means that one can skip the usual procedure of multiplying the time-domain signal by an increasing exponential function before replicating the FID and Fourier transforming it. However, replication of a single rotor period of evolution has been shown to lead to artifacts from correlated noise (*46*). Although these effects are generally minor, we chose to avoid them by simply acquiring several (usually ~5) rotor periods worth of evolution in t_1 (with the rotor period not necessarily being a multiple of the t_1 step). The FID was then multiplied with a Gaussian damping function to eliminate truncation artifacts. It is important to realize that the linewidths in all of the experimental spectra shown in this paper are almost entirely generated by the data-processing procedure and do not reflect true relaxation. For applications in which sensitivity is limited, however, it would be possible to collect a RELM spectrum with very few t_1 slices (one rotor period of evolution).

To demonstrate the possibility of applying RELM to a natural-abundance sample, experiments have been performed on L-tyrosine · HCl. Figure 5 shows a contour plot of the 2D RELM spectrum for $\omega_R/(2\pi) = 25$ kHz and $N_{enc1} = N_{enc2} = 2$ along with the RELM sideband pattern for one of the carbons. The carbon assignments are given in Ref. (*11*), and Table 2 lists the C–H distances for the methine and the phenylene carbons as determined from fits of the RELM sideband patterns. The spectrum shown in Fig. 5 took approximately 2 days to acquire. As the sideband pattern shows, the signal-to-noise ratio is quite high; a satisfactory spectrum could have been obtained in less time. Because this experiment started with carbon magnetization (from cross polarization), all of the carbons in L-tyrosine · HCl contribute to the directly detected signal. This contrasts with polarization-transfer methods (*11, 47*) where signal from carbons that are not directly bound to protons is not observed at short recoupling times. In fact, the carbons without nearby protons produce strong, albeit uninteresting, signals in the RELM experiment since they do not undergo significant dipolar dephasing.

Unlike in a previous heteronuclear double-quantum experiment (*11*), there is nothing intrinsic about the dipolar couplings in methylene groups that prevents sideband patterns from being recorded. However, the strong homonuclear coupling between the protons causes rapid relaxation, and the signal-to-noise for the methylene group in the experiment of Fig. 5 was significantly poorer than that for the methine groups. Furthermore, density matrix simulations (data not shown) demonstrated that the combination of finite pulse lengths and strong homonuclear coupling (of nearly the same magnitude as the spinning fre-

TABLE 2
C–H Bond Lengths as Determined from the RELM Spectrum of L-Tyrosine · HCl (see Fig. 5)

Atom	Distance (Å)
C2	1.16 ± 0.05
C5	1.13 ± 0.03
C6	1.12 ± 0.02
C7	1.13 ± 0.03
C8	1.15 ± 0.05

Note. Peak assignments are given in Fig. 5.

quency) significantly damps the higher-order sideband intensities, and this effect was confirmed experimentally. No attempt was, therefore, made to fit the sideband pattern for the methylene carbon.

So far, we have considered only directly bound protons in our fits of sideband patterns. However, as mentioned under Theory, the time-domain RELM signal acquires a pair of cosine factors for each proton in the sample, and thus RELM sideband patterns are potentially sensitive to remote-spin effects. Analytical simulations, which used proton geometries obtained from diffraction studies, were, therefore, performed to assess the effects of these remote spins, and it was found that when directly bound species are present, remote spins do not significantly perturb the relative sideband intensities. This explains the good agreement between the experiments and the spin-pair simulations.

The heteronuclear RELM technique has obvious similarities with the REDOR experiment. Of course, the recoupling mechanism in REDOR and RELM is exactly the same; what differs is the way in which the dipolar coupling information appears: either as a build-up curve of difference-spectra intensities as a function of recoupling time or as a sideband pattern recorded for a specific recoupling time.

In order to extract a reliable dipolar coupling for a spin pair from a RELM experiment, it is necessary to recouple long enough so that both ± 2 and ± 4 sidebands appear. The total number of recoupling periods, $N_{\mathrm{enc1}} + N_{\mathrm{enc2}}$, necessary to produce such a spectrum corresponds roughly with the position of the first minimum in the REDOR curve (see Appendix). Thus, for any case where REDOR oscillations can be seen, the RELM experiment can be performed. RELM experiments using over 30 rotor periods of recoupling (in each encoding segment) have already successfully been performed for a non-directly bound C–H pair (*48*), and longer encoding times should also be possible.

It is difficult to say whether REDOR or RELM can be performed in a shorter experimental time. At high spinning frequencies, only a few t_1 slices are needed to obtain a RELM spectrum. For instance, a pattern comparable to the one shown in Fig. 4a could have been obtained by acquiring 10 t_1 points with an increment of 3.33 μs at a spinning frequency of 30 kHz. The minimum number of slices required for a REDOR experiment is not so well defined, but it is probably similar. One must keep in mind that each point on a REDOR build-up curve is generated from the difference of two separate experiments, and nearly all REDOR build-up curves published to date have at least five points on them. Since the REDOR signal is generally concentrated in centerbands while the RELM intensity is necessarily spread out over sidebands, one might assume that fewer scans are needed for a REDOR experiment. However, the subtraction procedure required for REDOR decreases the signal while increasing the noise. It is, therefore, hard to quantify whether REDOR or RELM is more efficient.

One advantage of RELM over conventional REDOR is that one does not have to worry about background signals from uncoupled *S* spins. This is because the signal from any *S* spin that is not coupled to an *I* spin will contribute only to the centerband intensity, and the centerband intensity is neglected in RELM fits. The same advantage is obtained from a two-dimensional version of REDOR, the e*x*tended *d*ipolar *m*odulation (XDM) experiment (*24, 49*), in which the positions of the 180° pulses are systematically varied to generate sideband patterns. However, the dipolar sideband patterns in the XDM experiment, although scaled, retain the shape of the conventional MAS dipolar sideband pattern. This contrasts strongly with the RELM experiment, where very different sideband patterns can be generated by choosing different values of $N_{\mathrm{enc}} D_{IS}/\omega_{\mathrm{R}}$ (see Figs. 4a and 4b). It should be noted that the *t*ransferred-*e*cho *do*uble *r*esonance (TEDOR) (*50, 51*) experiment also circumvents the problem of uncoupled spins; a rotor-encoding analog of the TEDOR experiment has been introduced recently (*11*) and will be discussed in more detail in a separate publication (*47*).

Heteronuclear RELM with $N_{enc1} \neq N_{enc2}$

Conventionally, multiple-quantum experiments have been performed subject to the constraint $|\mathcal{H}_{\mathrm{rec}}\tau_{\mathrm{rec}}| = |\mathcal{H}_{\mathrm{exc}}\tau_{\mathrm{exc}}|$ (*19, 52*). Such pulse sequences lead to efficient reconversion of the multiple-quantum coherences into longitudinal magnetization. Furthermore, it is common to set $|\mathcal{H}_{\mathrm{rec}}| = |\mathcal{H}_{\mathrm{exc}}|$ so that the durations of the excitation and reconversion sequences are equal (*7, 53*).

However, in the case of the RELM experiment, there is no *a priori* reason to set $N_{\mathrm{enc1}} = N_{\mathrm{enc2}}$ since no coherences are being reconverted during the second half of the experiment. (Even in experiments where coherences are being reconverted, N_{enc1} and N_{enc2} do not necessarily have to be equal (*47, 50, 51*).) It is, therefore, of interest to explore what happens when $N_{\mathrm{enc1}} \neq N_{\mathrm{enc2}}$.

As discussed above, the Fourier transformation of Eq. [4] leads to a sideband pattern where only even-order sidebands are present. The intensities of these sidebands are determined by integrals of products of Bessel functions (see Appendix, Eq. [A4]), and the arguments of the Bessel functions depend on the parameters $N_{\mathrm{enc1}} D_{IS}/\omega_{\mathrm{R}}$ and $N_{\mathrm{enc2}} D_{IS}/\omega_{\mathrm{R}}$. For the case $N_{\mathrm{enc1}} = N_{\mathrm{enc2}}$, these sidebands necessarily have positive intensity (as shown in the Appendix), but for $N_{\mathrm{enc1}} \neq N_{\mathrm{enc2}}$ both positive and negative intensity sidebands are possible.

By using Eq. [A4] or by performing analytical simulations of the Fourier transform of Eq. [4], it is possible to identify combinations of encoding durations that produce negative-intensity sidebands for a given dipolar coupling strength. Figure 6a shows an experimental RELM pattern for the α carbon in L-alanine with $N_{\mathrm{enc1}} = 2$, $N_{\mathrm{enc2}} = 1$, and $\omega_{\mathrm{R}}/(2\pi) = 19.4$ kHz. The intensities of the ± 2 sidebands are clearly negative. The best-fit simulation (in which, as usual, the centerband intensity is not included in the fit) corresponds to a C–H distance of 1.10 ± 0.01 Å.

As the spinning frequency is increased, the magnitudes of

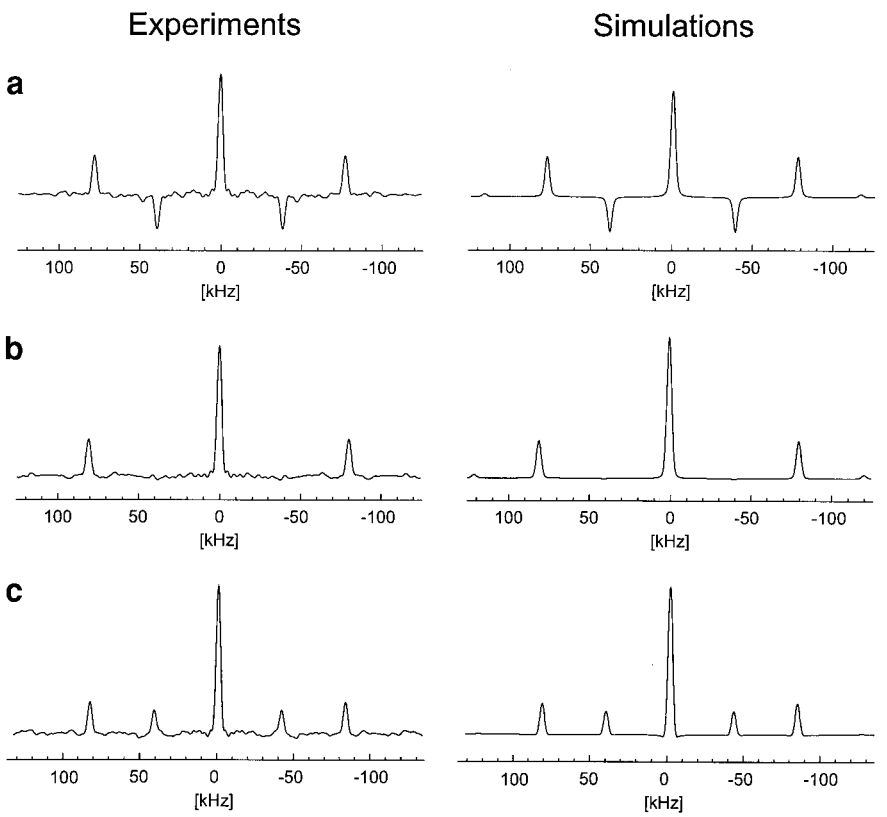

FIG. 6. ^{1}H–^{13}C RELM spectra of the methine carbon in L-alanine with $N_{enc1} = 2$ and $N_{enc2} = 1$. The experimental spectra (recorded on a 300-MHz spectrometer) are on the left side of the figure and the best-fit simulations are on the right side. Centerband intensities were not included in the fit. (a) For $\omega_R/(2\pi) = 19.4$ kHz the ± 2 sidebands are clearly negative, (b) for $\omega_R/(2\pi) = 20.1$ kHz the ± 2 sidebands have zero intensity, and (c) for $\omega_R/(2\pi) = 20.8$ kHz the ± 2 sidebands are positive.

the negative-intensity sidebands decrease and eventually reach zero. Upon further increase of the spinning frequency, the sidebands reappear but this time with positive intensity. The zero crossing occurs at a spinning frequency of approximately 20.1 kHz, and the best fit to the zero-crossing spectrum corresponds to an internuclear distance of 1.11 ± 0.01 Å (see Fig. 6b). Figure 6c shows a spectrum recorded at a spinning frequency of 20.8 kHz. Although the excitation and reconversion periods are still unequal, all sidebands are now positive. The best-fit distance is 1.12 ± 0.02 Å in this case.

The parameter space describing the intensities of the various sideband orders as a function of $N_{enc1}D_{IS}/\omega_R$ and $N_{enc2}D_{IS}/\omega_R$ is complicated due to the many zero crossings of the Bessel functions, and it is not possible to provide simple "rules of thumb" for determining which pair (or pairs) of sidebands will be inverted under which conditions. However, for a given set of conditions the sideband intensities can easily be calculated using the information provided in the Appendix.

In principle, zero crossings could provide a very sensitive measure of internuclear distances, but the sideband patterns for encoding periods of unequal length might be more affected by spectrometer imperfections than the patterns for equal-length encoding periods. When the $N_{enc1} \neq N_{enc2}$ RELM experiment was performed on one of our spectrometers (the DRX-700), phase distortions of the outer sidebands were sometimes observed (data not shown). For symmetric versions of the RELM experiment, no phase distortions were observed on either spectrometer, and identical sideband patterns could be recorded. It is also unclear why the best-fit distances extracted from the experiments of Fig. 6 are slightly shorter than those determined from the experiments in Figs. 4a and 4b (although they are still probably within the experimental error).

Homonuclear RELM

To demonstrate the possibility of performing RELM on homonuclear spin systems, spectra of trichloroacetic acid were recorded using the pulse sequence of Fig. 3. As mentioned earlier, homonuclear RELM using the BABA sequence can only produce easily interpretable spectra for the case of effectively isolated spin pairs with minor chemical-shielding anisotropy. Trichloroacetic acid fulfills the first of these conditions; a single-crystal neutron diffraction study showed that it, like many other acetic acids, crystallizes in dimer pairs, with the protons being 2.457 Å apart (*54*). While the proton chemical-shielding anisotropy is not small ($\Delta\sigma^{CS} = 13.5$ ppm), the relative orientation of the CSA and dipolar tensors has previously been determined from a single-crystal NMR study (*55*).

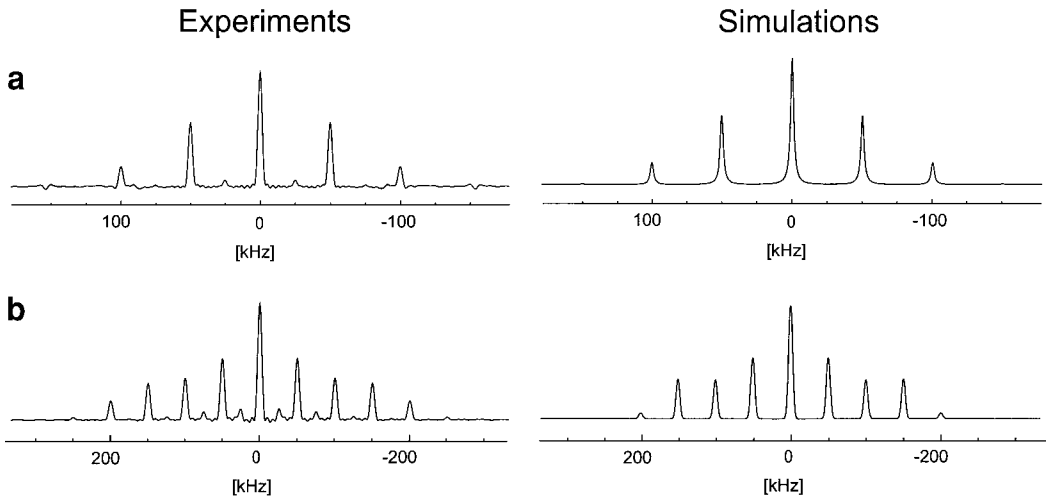

FIG. 7. Homonuclear ^{1}H RELM spectra of trichloroacetic acid. The experimental spectra (recorded on a 700-MHz spectrometer) are on the left side of the figure and the best-fit simulations are on the right side. (a) $\omega_R/(2\pi) = 25$ kHz and $N_{enc1} = N_{enc2} = 4$ and (b) $\omega_R/(2\pi) = 25$ kHz and $N_{enc1} = N_{enc2} = 8$.

Figure 7 shows homonuclear ^{1}H RELM spectra of trichloroacetic acid for two different excitation times. The spectra were fit to the Fourier transform of Eq. [11], and the centerband intensity was excluded from the fits. The distances extracted from the fits were 2.67 $\pm$ 0.04 and 2.79 $\pm$ 0.02 Å for Figs. 7a and 7b, respectively. These distances differ quite significantly from 2.457 Å, but there are several possible explanations. First, as mentioned above, internuclear distances measured by NMR are known to be slightly longer than distances measured by diffraction (*43–45*). Second, many carboxylic acid dimers are known to undergo complicated motion, including tunneling (at low temperatures) and two-site jumps (at higher temperatures) (*56–58*). The possibility of such dynamics was neglected in this analysis although, if present, a two-site jump would lead to an averaging of the dipolar tensors corresponding to each tautomer and, thus, the static two-spin approximation would not be strictly applicable. Third, the chemical-shielding anisotropy is not small (*55*), and the BABA recoupling sequence is sensitive to chemical-shielding effects. Due to all of these factors, the distance extracted from the RELM measurements cannot be considered to be highly accurate, but the data shown in Fig. 7 do demonstrate that rotor encoding of longitudinal magnetization is possible in the homonuclear case.

Unlike the heteronuclear RELM spectra presented in the previous sections, the experimental spectra in Fig. 7 show small sidebands of the "wrong" (i.e., odd) order. The origin of these sidebands cannot be precession under the chemical-shielding or dipolar interaction during t_1 because such precession does not occur in the RELM experiment. However, density-matrix simulations show that slight misadjustments of the pulse length (by $\sim$0.2 μs for the RF field strength and spinning frequency used in this experiment) can lead to small odd-order sidebands even for an isolated spin pair with no chemical-shielding anisotropy and no resonance offset. Fortunately, the simulations also show that the presence of such sidebands does not significantly distort the relative intensities of the even-order peaks.

To estimate the extent to which CSA effects perturb the spectra of trichloroacetic acid, density-matrix simulations were performed for an isolated pair of protons. The internuclear distance was set to 2.66 Å, and eight rotor cycles of the compensated BABA sequence at a spinning frequency of 25.0 kHz were used for each encoding period. Figure 8a shows the simulated RELM spectrum for the case of no CSA whereas Fig. 8b shows the simulated RELM spectrum when the CSA parameters are included (*55*). Although the chemical-shielding anisotropy parameter for trichloroacetic acid is only 13.5 ppm, this corresponds to 9.45 kHz for protons at a Larmor frequency of 700.1 MHz. Thus, it is approximately 50% larger than the dipolar coupling between the spins. A comparison of Figs. 8a and 8b shows that the chemical-shielding anisotropy does influence the relative intensities of the peaks; in particular, the CSA damps the intensities of the outer sidebands relative to the $\pm$2 sidebands. Nonetheless, the number of sidebands and the general features of the pattern (i.e., the $\pm$6 sidebands being more intense than the $\pm$4) remain the same.

In contrast, homonuclear RELM spectra can be profoundly altered when the chemical-shielding anisotropy parameter greatly exceeds the dipolar coupling between the spins. As an example, Fig. 8c shows a simulated homonuclear RELM pattern for a pair of ^{31}P nuclei that are 2.925 Å apart and have no CSA. Eight cycles of BABA recoupling at a spinning frequency of 29.4 kHz were used for each encoding period, leading to a RELM pattern with small $\pm$4 sidebands. This pattern represents the lower threshold of patterns that could be fit if the centerband intensity is to be ignored. Figure 8d shows a simulation which uses the same conditions as those in Fig. 8c except that the CSA parameters of $Na_4P_2O_7 \cdot 10H_2O$ are now included (*59*). This large CSA (15.3 kHz at a static field strength of 11.7 T) leads to nearly complete suppression of the

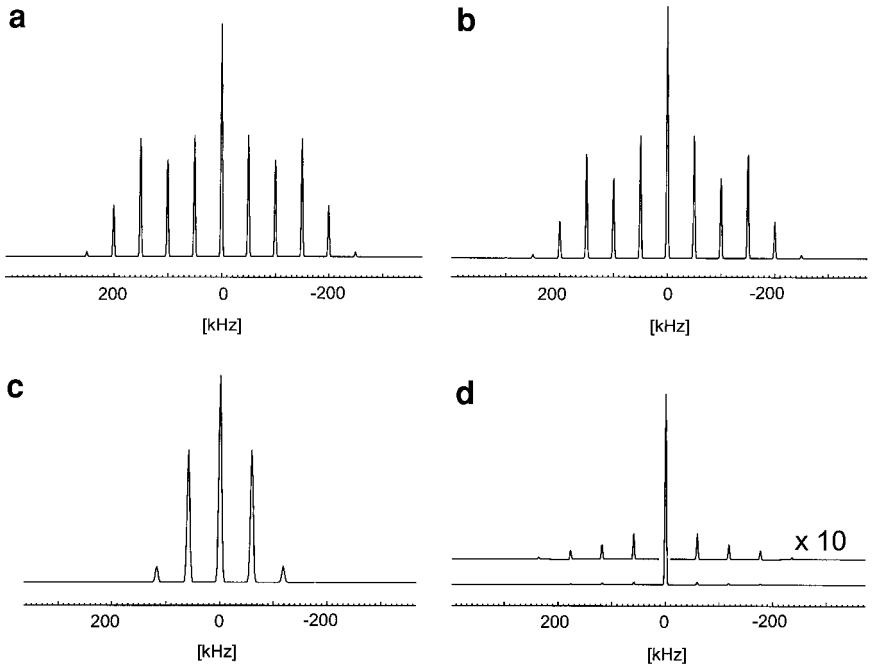

FIG. 8. Simulations of homonuclear RELM spectra with and without chemical-shielding anisotropy. The four-rotor cycle, offset-compensated BABA sequence was used in all cases. Ideal (zero-width) pulses were applied on resonance, and the step size of the calculations was 500 ns. (a) Simulation of ^{1}H–^{1}H RELM for trichloroacetic acid with the chemical-shielding anisotropy neglected. The parameters used were $\omega_R/(2\pi) = 25$ kHz, $N_{enc1} = N_{enc2} = 8$, and $D_{II}/(2\pi) = 6339$ Hz. (b) Simulation of ^{1}H–^{1}H RELM for trichloroacetic acid with the chemical-shielding anisotropy (at 700 MHz) included. The CSA parameters used were based on those found in Ref. (*55*) with $\Delta\sigma_{CS} = 13.5$ ppm, $\eta_{CS} = 0.067$, and the Euler angles of the principal-axes system of the CSA relative to the dipolar axis being set to ($\alpha_{CS} = 270°$, $\beta_{CS} = 100°$) for both spins. All other parameters were the same as those in (a). (c) Simulation of ^{31}P–^{31}P RELM for $Na_4P_2O_7 \cdot 10H_2O$ with the chemical-shielding anisotropy neglected. Relevant parameters were $\omega_R/(2\pi) = 29.4$ kHz, $N_{enc1} = N_{enc2} = 8$, and $D_{II}/(2\pi) = 787$ Hz. (d) Simulation of ^{31}P–^{31}P RELM for $Na_4P_2O_7 \cdot 10H_2O$ with the chemical-shielding anisotropy (at 500 MHz ^{1}H frequency) included. The CSA parameters used were based on those found in Ref. (*59*) with $\Delta\sigma_{CS} = 75.6$ ppm, $\eta_{CS} = 0.216$, and the Euler angles of the principal-axes system of the CSA relative to the dipolar axis being ($\alpha_{CS} = 100.773°$, $\beta_{CS} = 157.375°$, $\gamma_{CS} = 259.071°$) for one of the spins and ($\alpha_{CS} = 100.773°$, $\beta_{CS} = 22.725°$, $\gamma_{CS} = 280.929°$) for the other spin. All other parameters were the same as those in (c).

sidebands relative to the centerband. Furthermore, even if the sensitivity of the spectrometer were great enough to allow these sidebands to be observed (which is unlikely), their number and relative intensities do not correspond with those of Fig. 8c.

In cases (such as this) where the CSA is significantly greater than the dipolar coupling, the RELM sideband patterns will be sensitive to the relative orientation of the CSA and dipolar tensors although for some orientations the patterns may not be so deleteriously affected. Unfortunately, the relative orientations of the CSA and dipolar tensors is often not known and can be difficult to measure. It is beyond the scope of this paper to explore the dependence of sideband intensities on CSA magnitudes and orientations, but as Fig. 8 makes clear, one must proceed with caution in the case of large chemical-shielding anisotropies. Similar caution is also required when analyzing sideband patterns from double-quantum experiments which use the BABA sequence on nuclei other than ^{1}H; protons represent a special case because their dipolar couplings are strong and their chemical-shielding anisotropies are relatively small.

CONCLUSIONS

The experimental results presented above demonstrate that rotor encoding of longitudinal magnetization can be used to generate spinning-sideband patterns with intensities that are determined by the properties of the pulse sequences used for the encoding. The effective Hamiltonians for these pulse sequences must depend on the phase of the rotor (i.e., the Euler angle γ), but the two encoding periods need not be identical. In fact, by choosing encoding periods of unequal length, it is possible to generate negative-intensity sidebands in certain cases. Such sideband patterns are extremely sensitive to the strength of the dipolar coupling and, therefore, can provide valuable structural information.

While homonuclear RELM sideband patterns can easily be generated, they suffer from the drawback that the homonuclear recoupling sequences developed to date also recouple part of the chemical-shielding anisotropy. This is particularly true of the laboratory-frame sequences which have the necessary rotor-phase dependence for rotor encoding. Even when such sequences are designed such that their zeroth-order average

Hamiltonians (assuming perfect δ pulses) do not depend on the CSA (*22, 60*), they are still too sensitive to residual chemical-shielding effects to generate easily interpretable sideband patterns for nuclei, such as ^{31}P, which have large CSAs. For such nuclei, rotor-synchronized multiple-quantum build-up curves (which rely on total intensities rather than sideband patterns) are a better alternative for distance determination (*61, 62*). However, the homonuclear RELM experiment should be applicable to protons with their typically small CSA values.

The heteronuclear RELM experiment presented above is far more versatile. The REDOR recoupling sequence refocuses the chemical-shielding anisotropy; therefore, the sideband patterns obtained are purely dipolar. This contrasts with previously presented heteronuclear double-quantum experiments (*10, 11*) in which the sideband patterns were influenced by chemical-shielding evolution during t_1. Although the experiments presented in this paper were restricted to protons and carbons, the heteronuclear RELM experiment can easily be modified to measure internuclear distances between two rare nuclei such as ^{13}C and ^{15}N, as is commonly done in REDOR experiments. Since proton coupling effects could then be eliminated by radiofrequency decoupling, the high spinning frequencies used in this paper would no longer be necessary, and the MAS frequencies typically used in REDOR experiments (a few kHz) should suffice.

Both REDOR and RELM measure heteronuclear dipolar coupling constants, but they do so in different ways, with the REDOR experiment probing total intensity as a function of recoupling time and the RELM experiment generating a sideband pattern for a given recoupling time. Although heteronuclear sideband patterns can also be generated by other techniques such as XDM (*24, 49*), rotor-encoding-based methods provide the experimentalist with an unprecedented degree of control over the appearance of the sideband pattern. A variety of spinning-sideband patterns (with spectral widths approaching 1 MHz) can be generated at a single spinning frequency, and negative sidebands can also be created.

While the heteronuclear RELM experiment has the advantage of generating sideband patterns that are free of chemical-shift effects, it also has the corresponding disadvantage that site resolution in the proton dimension is not available. In contrast, heteronuclear double-quantum experiments allow one to determine which types of protons are in the vicinity of a given type of carbon (*10, 11, 47*). Furthermore, multiple-quantum experiments can be used as filters to select minimum cluster sizes whereas the direct dimension of the RELM experiment will contain signals from both coupled and uncoupled spins. For a thorough examination of a given system, a combination of approaches will likely be desirable, and an in-depth investigation of a variety of heteronuclear experiments (involving multiple-quantum coherences, dipolar order, transverse magnetization, and antiphase terms) is the subject of a forthcoming publication (*47*).

A potential advantage of sideband approaches such as RELM, as compared to build-up curves, is that it may be possible to incorporate them into multidimensional correlation experiments. Furthermore, sideband patterns could also possibly be used to study motional averaging effects and local topologies. Such studies are currently underway in our group.

APPENDIX

Under Results and Discussion, a series of spectra was presented where the intensities of the ± 2 sidebands went through a zero crossing as the spinning frequency was varied. To understand how such zero crossings originate, it is useful to examine the intensities of the spinning sidebands in more detail. When the RELM experiment of Fig. 2 is applied to an isolated heteronuclear spin pair, the time-domain signal has the following form (see Eqs. [2] and [4]),

$$\begin{aligned} S(t_1;\, t_2 = 0) &= \frac{1}{4\pi}\int_0^{2\pi} d\gamma_{IS} \int_0^{\pi} \sin\beta_{IS} d\beta_{IS} \\ &\times \cos\left(N_{\mathrm{enc1}} \frac{D_{IS}}{\omega_{\mathrm{R}}} 2\sqrt{2} \sin 2\beta_{IS} \sin\gamma_{IS} \right) \\ &\times \cos\left(N_{\mathrm{enc2}} \frac{D_{IS}}{\omega_{\mathrm{R}}} 2\sqrt{2} \sin 2\beta_{IS} \sin(\omega_{\mathrm{R}} t_1 + \gamma_{IS}) \right), \end{aligned} \quad [A1]$$

where the powder averaging over the Euler angles β_{IS} and γ_{IS} has been explicitly included. Substituting Eq. [5] into Eq. [A1], regrouping, and using the relation $\cos(\theta + \phi) = \cos\theta \cdot \cos\phi - \sin\theta \cdot \sin\phi$ lead to

$$\begin{aligned} S(t_1;\, t_2 = 0) &= \frac{1}{4\pi}\int_0^{2\pi} d\gamma_{IS} \int_0^{\pi} \sin\beta_{IS} d\beta_{IS} \Big[J_0(u) J_0(v) \\ &+ 2J_0(v) \sum_{k=1}^{\infty} J_{2k}(u) \cos(2k\gamma_{IS}) + 2J_0(u) \sum_{n=1}^{\infty} J_{2n}(v) \\ &\times \{ \cos(2n\gamma_{IS}) \cos(2n\omega_{\mathrm{R}} t_1) - \sin(2n\gamma_{IS}) \sin(2n\omega_{\mathrm{R}} t_1) \} \\ &+ 4 \sum_{n=1}^{\infty} \sum_{k=1}^{\infty} J_{2k}(u) J_{2n}(v) \cos(2k\gamma_{IS}) \{ \cos(2n\gamma_{IS}) \\ &\times \cos(2n\omega_{\mathrm{R}} t_1) - \sin(2n\gamma_{IS}) \sin(2n\omega_{\mathrm{R}} t_1) \} \Big], \end{aligned} \quad [A2]$$

where $u = (N_{\mathrm{enc1}} D_{IS}/\omega_{\mathrm{R}}) 2\sqrt{2} \sin 2\beta_{IS}$ and $v = (N_{\mathrm{enc2}} D_{IS}/\omega_{\mathrm{R}}) 2\sqrt{2} \sin 2\beta_{IS}$. After integration over γ_{IS}, most of the terms in Eq. [A2] vanish. However, the integral over $\cos(2k\gamma_{IS})\cos(2n\gamma_{IS})$ is nonvanishing for the case in which k and n are equal. Thus, Eq. [A2] simplifies to

$$S(t_1;\, t_2 = 0) = \int_0^{\pi} \left[\frac{1}{2} J_0(u)J_0(v) + \sum_{n=1}^{\infty} J_{2n}(u)J_{2n}(v)\cos(2n\omega_R t_1) \right] \times \sin\beta_{IS} d\beta_{IS}. \quad [A3]$$

Since $\cos(2n\omega_R t_1) = (e^{i2n\omega_R t_1} + e^{-i2n\omega_R t_1})/2$, it is clear that the intensities of the $\pm 2 \cdot n$ sidebands are proportional to

$$I_{\pm 2n} = \frac{1}{2} \int_0^{\pi} J_{2n}\left(N_{\text{encl}} \frac{D_{IS}}{\omega_R} 2\sqrt{2} \sin 2\beta_{IS} \right) \times J_{2n}\left(N_{\text{enc2}} \frac{D_{IS}}{\omega_R} 2\sqrt{2} \sin 2\beta_{IS} \right) \sin\beta_{IS} d\beta_{IS}. \quad [A4]$$

Equation [A4] can be easily evaluated using a computer. Figure 9a shows the intensity of the ± 2 sidebands (calculated from Eq. [A4]) as a function of the spinning frequency for $N_{\text{encl}} = 2$, $N_{\text{enc2}} = 1$, and $D_{IS}/(2\pi) = 21{,}990$ Hz. These conditions correspond to those used in the experiments of Fig. 6, and the presence of the zero crossing at approximately 20.1 kHz is readily apparent. Analogous curves can be constructed for other sideband orders, dipolar coupling strengths, and recoupling durations.

When $N_{\text{encl}} = N_{\text{enc2}} \equiv N_{\text{enc}}$, Eq. [A4] simplifies to

$$\frac{1}{2} \int_0^{\pi} \left[J_{2n}\left(N_{\text{enc}} \frac{D_{IS}}{\omega_R} 2\sqrt{2} \sin 2\beta_{IS} \right) \right]^2 \sin\beta_{IS} d\beta_{IS}. \quad [A5]$$

Since $\sin(\beta_{IS})$ is positive over the range 0 to π, it is clear that Eq. [A5] can never be negative. Thus, when the number of excitation and reconversion periods is equal, only sidebands with positive intensity are obtained. Figure 9b shows the theoretical relative intensities for the centerband and the ± 2, ± 4, ± 6, and ± 8 sidebands for this case. The total RELM intensity is given by

$$I_{\text{RELM}} = I_0 + 2 \sum_{n=1}^{\infty} I_{\pm 2n} \quad [A6]$$

since the sidebands are symmetric (i.e., $I_{+2n} = I_{-2n} \equiv I_{\pm 2n}$). As can be seen from the inset in Fig. 9b, the total RELM intensity as a function of increasing encoding time starts at 1.0, decays monotonically toward 0.5, and then oscillates about 0.5. This behavior results from the cosine–cosine form of the RELM modulation (see Eqs. [4] and [11]) and is the counterpart to the previously simulated sine–sine-modulated double-quantum build-up curves (*7*) which start at zero intensity but also eventually oscillate about the limit of 0.5. In practice, of course, transverse relaxation during the encoding periods causes the intensity at long recoupling times to decay toward zero in both experiments. For encoding periods of unequal length ($N_{\text{encl}} \neq N_{\text{enc2}}$), the total RELM intensity decays to values lower than 0.5 even when relaxation effects are neglected.

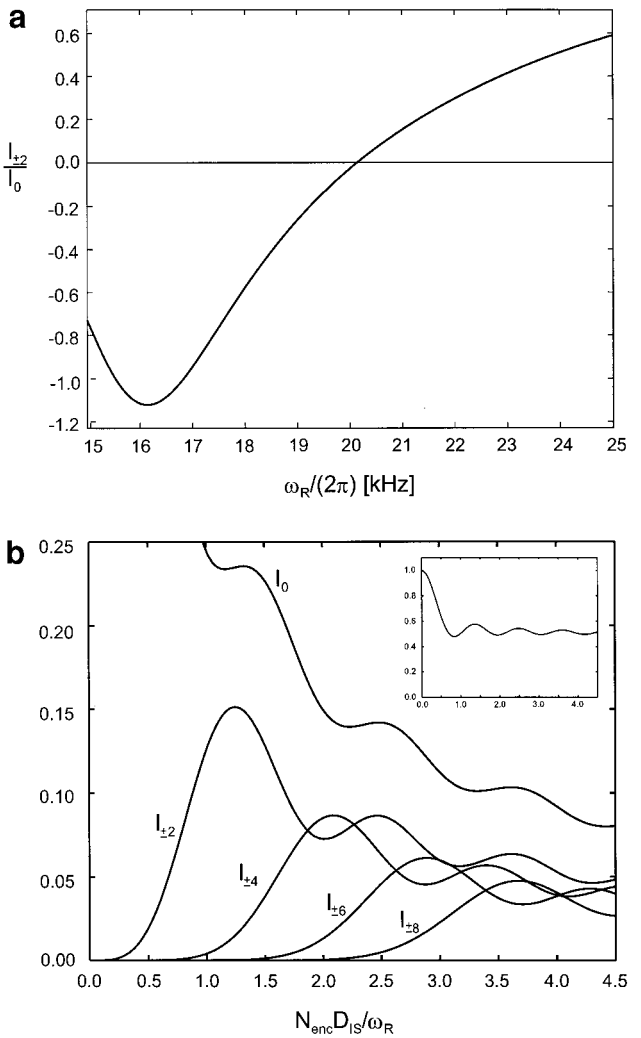

FIG. 9. (a) Intensity of the ± 2 sidebands (normalized to the centerband) as a function of the spinning frequency for the experiment of Fig. 2 with $N_{\text{encl}} = 2$, $N_{\text{enc2}} = 1$, and $D_{IS}/(2\pi) = 21{,}990$ Hz. A crossover from negative to positive intensity occurs at a spinning frequency of approximately 20.1 kHz. (b) Intensities of the centerband and the ± 2, ± 4, ± 6, and ± 8 sidebands as a function of the product of the excitation time and dipolar coupling strength for the experiment of Fig. 2 with $N_{\text{encl}} = N_{\text{enc2}} \equiv N_{\text{enc}}$. The inset depicts the total intensity of the RELM experiment, which was calculated using Eq. [A6] and truncating after $n = 7$.

To obtain an accurate measure of the internuclear distance (i.e., by neglecting the centerband), it is necessary that both ± 2 and ± 4 sidebands be generated. As can easily be seen from Fig. 9b, this condition corresponds to $(N_{\text{enc}} D_{IS}/\omega_R) \approx 1.5$. Since two encoding periods are needed for the RELM experiment, the total recoupling duration is given by $(2N_{\text{enc}}\tau_R) \approx 3 \cdot (2\pi/D_{IS})$. Comparison with the universal REDOR curve (*63*) shows that this amount of recoupling approximately equals the

amount of recoupling necessary for $\Delta S/S_0$ to reach its first local minimum in a conventional REDOR experiment.

ACKNOWLEDGMENTS

We thank Ute Pawelzik for crystallizing the L-tyrosine · HCl, Dr. Gunnar Jeschke for helping with MATLAB, and Drs. Steven Brown and Matthias Ernst for commenting on the manuscript. Helpful discussions with Professor Dan E. Demco in the early stages of this project are gratefully acknowledged. S.M.D. thanks the United States National Science Foundation for an NSF–NATO postdoctoral fellowship. The authors are grateful to the Deutsche Forschungsgemeinschaft (SFB262) for financial support.

REFERENCES

1. E. R. Andrew, The narrowing of NMR spectra of solids by high-speed specimen rotation and the resolution of chemical shift and spin multiplet structures for solids, *Prog. NMR Spectrosc.* **8,** 1–39 (1971).
2. M. M. Maricq and J. S. Waugh, NMR in rotating solids, *J. Chem. Phys.* **70,** 3300–3316 (1979).
3. J. Herzfeld and A. E. Berger, Sideband intensities in NMR spectra of samples spinning at the magic angle, *J. Chem. Phys.* **73,** 6021–6030 (1980).
4. C. Filip, S. Hafner, I. Schnell, D. E. Demco, and H. W. Spiess, Solid-state nuclear magnetic resonance spectra of dipolar-coupled multi-spin systems under fast magic-angle spinning, *J. Chem. Phys.* **110,** 423–440 (1999).
5. H. Geen, J. J. Titman, J. Gottwald, and H. W. Spiess, Solid-state proton multiple-quantum NMR spectroscopy with fast magic angle spinning, *Chem. Phys. Lett.* **227,** 79–86 (1994).
6. J. Gottwald, D. E. Demco, R. Graf, and H. W. Spiess, High-resolution double-quantum NMR spectroscopy of homonuclear spin pairs and proton connectivities in solids, *Chem. Phys. Lett.* **243,** 314–323 (1995).
7. R. Graf, D. E. Demco, J. Gottwald, S. Hafner, and H. W. Spiess, Dipolar couplings and internuclear distances by double-quantum nuclear magnetic resonance spectroscopy of solids, *J. Chem. Phys.* **106,** 885–895 (1997).
8. U. Friedrich, I. Schnell, D. E. Demco, and H. W. Spiess, Triple-quantum NMR spectroscopy in dipolar solids, *Chem. Phys. Lett.* **285,** 49–58 (1998).
9. U. Friedrich, I. Schnell, S. P. Brown, A. Lupulescu, D. E. Demco, and H. W. Spiess, Spinning-sideband patterns in multiple-quantum magic-angle spinning NMR spectroscopy, *Mol. Phys.* **95,** 1209–1227 (1998).
10. K. Saalwächter, R. Graf, D. E. Demco, and H. W. Spiess, Heteronuclear double-quantum MAS NMR spectroscopy in dipolar solids, *J. Magn. Reson.* **139,** 287–301 (1999).
11. K. Saalwächter, R. Graf, and H. W. Spiess, Recoupled polarization transfer heteronuclear ^{1}H–^{13}C multiple-quantum correlation in solids under ultra-fast MAS, *J. Magn. Reson.* **140,** 471–476 (1999).
12. L. Marinelli and L. Frydman, On the origin of spinning sidebands in MQMAS NMR experiments, *Chem. Phys. Lett.* **275,** 188–198 (1997).
13. J.-P. Amoureux, M. Pruski, D. P. Lang, and C. Fernandez, The effect of RF power and spinning speed on MQMAS NMR, *J. Magn. Reson.* **131,** 170–175 (1998).
14. T. Charpentier, C. Fermon, and J. Virlet, Numerical and theoretical analysis of multiquantum magic-angle spinning experiments, *J. Chem. Phys.* **109,** 3116–3130 (1998).
15. A. F. de Jong, A. P. M. Kentgens, and W. S. Veeman, Two-dimensional exchange NMR in rotating solids: A technique to study very slow molecular reorientations, *Chem. Phys. Lett.* **109,** 337–342 (1984).
16. A. Hagemeyer, K. Schmidt-Rohr, and H. W. Spiess, Two-dimensional nuclear magnetic resonance experiments for studying molecular order and dynamics in static and in rotating solids, *Adv. Magn. Reson.* **13,** 85–130 (1989).
17. R. Tycko and A. E. Berger, Dual processing of two-dimensional exchange data in magic angle spinning NMR of solids, *J. Magn. Reson.* **141,** 141–147 (1999).
18. M. Schneider, D. E. Demco, and B. Blümich, ^{1}H NMR imaging of residual dipolar couplings in cross-linked elastomers: Dipolar-encoded longitudinal magnetization, double-quantum, and triple-quantum filters, *J. Magn. Reson.* **140,** 432–441 (1999).
19. R. R. Ernst, G. Bodenhausen, and A. Wokaun, "Principles of Nuclear Magnetic Resonance in One and Two Dimensions," 2nd ed., Clarendon Press, Oxford (1991).
20. T. Gullion and J. Schaefer, Rotational-echo double-resonance NMR, *J. Magn. Reson.* **81,** 196–200 (1989).
21. R. Tycko and G. Dabbagh, Double-quantum filtering in magic-angle-spinning NMR spectroscopy: An approach to spectral simplification and molecular-structure determination, *J. Am. Chem. Soc.* **113,** 9444–9448 (1991).
22. M. Feike, D. E. Demco, R. Graf, J. Gottwald, S. Hafner, and H. W. Spiess, Broadband multiple-quantum NMR spectroscopy, *J. Magn. Reson. A* **122,** 214–221 (1996).
23. Y. K. Lee, N. D. Kurur, M. Helmle, O. G. Johannessen, N. C. Nielsen, and M. H. Levitt, Efficient dipolar recoupling in the NMR of rotating solids. A sevenfold symmetric radiofrequency pulse sequence, *Chem. Phys. Lett.* **242,** 304–309 (1995).
24. T. Gullion and J. Schaefer, Detection of weak heteronuclear dipolar coupling by rotational-echo double-resonance nuclear magnetic resonance, *Adv. Magn. Reson.* **13,** 57–83 (1989).
25. A. E. Bennett, R. G. Griffin, and S. Vega, Recoupling of homo- and heteronuclear dipolar interactions in rotating solids, *NMR Basic Principles Prog.* **33,** 1–77 (1994).
26. M. Hong, J. D. Gross, and R. G. Griffin, Site-resolved determination of peptide torsion angle ϕ from the relative orientations of backbone N–H and C–H bonds by solid-state NMR, *J. Phys. Chem. B* **101,** 5869–5874 (1997).
27. C. A. Michal and L. W. Jelinski, REDOR 3D: Heteronuclear distance measurements in uniformly labeled and natural abundance solids, *J. Am. Chem. Soc.* **119,** 9059–9060 (1997).
28. M. Abramowitz and I. A. Stegun (Eds.), "Handbook of Mathematical Functions," Dover, New York (1972).
29. J. M. Goetz and J. Schaefer, REDOR dephasing by multiple spins in the presence of molecular motion, *J. Magn. Reson.* **127,** 147–154 (1997).
30. T. Terao, H. Miura, and A. Saika, Dipolar SASS NMR spectroscopy: Separation of heteronuclear dipolar powder patterns in rotating solids, *J. Chem. Phys.* **85,** 3816–3826 (1986).
31. C. Schmidt, K. J. Kuhn, and H. W. Spiess, Distribution of correlation times in glassy polymers from pulsed deuteron NMR, *Prog. Colloid Polym. Sci.* **71,** 71–76 (1985).
32. J. Schaefer, E. O. Stejskal, R. A. McKay, and W. T. Dixon, Molecular motion in polycarbonates by dipolar rotation spin-echo ^{13}C NMR, *Macromolecules* **17,** 1479–1489 (1984).
33. K. Saalwächter and K. Schmidt-Rohr, Relaxation-induced dipolar exchange with recoupling: An MAS NMR method for determining heteronuclear distances without irradiating the second spin, *J. Magn. Reson.,* in press.

34. H. W. Spiess, Rotation of molecules and nuclear spin relaxation, *NMR Basic Principles Prog.* **15,** 55–214 (1978).
35. A. E. Bennett, C. M. Rienstra, M. Auger, K. V. Lakshmi, and R. G. Griffin, Heteronuclear decoupling in rotating solids, *J. Chem. Phys.* **103,** 6951–6958 (1995).
36. W. H. Press, S. A. Teukolsky, W. T. Vetterling, and B. P. Flannery, "Numerical Recipes in C: The Art of Scientific Computing," 2nd ed., Cambridge Univ. Press, Cambridge (1992).
37. S. A. Smith, T. O. Levante, B. H. Meier, and R. R. Ernst, Computer simulations in magnetic resonance: An object-oriented programming approach, *J. Magn. Reson. A* **106,** 75–105 (1994).
38. V. B. Cheng, H. H. Suzakawa, Jr., and M. Wolfsberg, Investigations of a non-random numerical method for multidimensional integration, *J. Chem. Phys.* **59,** 3992–3999 (1973).
39. "Matlab Reference Guide," The Mathworks Inc., Natick, MA (1992).
40. M. S. Lehmann, T. F. Koetzle, and W. C. Hamilton, Precision neutron diffraction structure determination of protein and nucleic acid compounds. I. The crystal and molecular structure of the amino acid L-alanine, *J. Am. Chem. Soc.* **94,** 2657–2660 (1972).
41. M. Munowitz, W. P. Aue, and R. G. Griffin, Two-dimensional separation of dipolar and scaled isotropic chemical-shift interactions in magic-angle NMR spectra, *J. Chem. Phys.* **77,** 1686–1689 (1982).
42. J. Schaefer, R. A. McKay, E. O. Stejskal, and W. T. Dixon, Dipolar rotational spin-echo ^{13}C NMR of polymers, *J. Magn. Reson.* **52,** 123–129 (1983).
43. M. Linder, A. Höhener, and R. R. Ernst, Orientation of tensorial interactions determined from two-dimensional NMR powder spectra, *J. Chem. Phys.* **73,** 4959–4970 (1980).
44. E. R. Henry and A. Szabo, Influence of vibrational motion on solid state line shapes and NMR relaxation, *J. Chem. Phys.* **82,** 4753–4761 (1985).
45. T. Nakai, J. Ashida, and T. Terao, Influence of small-amplitude motions on two-dimensional powder patterns: Anisotropic vibrations in calcium formate, *Mol. Phys.* **67,** 839–847 (1989).
46. D. W. Alderman, G. McGeorge, J. Z. Hu, R. J. Pugmire, and D. M. Grant, A sensitive high resolution magic angle turning experiment for measuring chemical shift tensor principle values, *Mol. Phys.* **95,** 1113–1126 (1998).
47. K. Saalwächter, R. Graf, and H. W. Spiess, Recoupled polarization-transfer methods for solid–state ^{1}H–^{13}C heteronuclear correlation in the limit of fast MAS, in preparation.
48. S. M. De Paul, unpublished results.
49. T. Gullion, M. D. Poliks, and J. Schaefer, Extended dipolar modulation and magic-angle spinning, *J. Magn. Reson.* **80,** 553–558 (1988).
50. A. W. Hing, S. Vega, and J. Schaefer, Transferred-echo double-resonance NMR, *J. Magn. Reson.* **96,** 205–209 (1992).
51. A. W. Hing, S. Vega, and J. Schaefer, Measurement of heteronuclear dipolar coupling by transferred-echo double-resonance NMR, *J. Magn. Reson. A* **103,** 151–162 (1993).
52. W. S. Warren, S. Sinton, D. P. Weitekamp, and A. Pines, Selective excitation of double-quantum coherence in nuclear magnetic resonance, *Phys. Rev. Lett.* **43,** 1791–1794 (1979).
53. J. Baum, M. Munowitz, A. N. Garroway, and A. Pines, Multiple-quantum dynamics in solid-state NMR, *J. Chem. Phys.* **83,** 2015–2025 (1985).
54. P.-G. Jönsson and W. C. Hamilton, Hydrogen bond studies. LX. A single crystal neutron diffraction study of trichloroacetic acid dimer, *J. Chem. Phys.* **56,** 4433–4439 (1972).
55. C. R. Dybowski, B. C. Gerstein, and R. W. Vaughan, The proton chemical shift tensor in trichloroacetic acid, *J. Chem. Phys.* **67,** 3412–3415 (1977).
56. A. Stöckli, B. H. Meier, R. Kreis, R. Meyer, and R. R. Ernst, Hydrogen bond dynamics in isotopically substituted benzoic acid dimers, *J. Chem. Phys.* **93,** 1502–1520 (1990).
57. A. Heuer and U. Haeberlen, The dynamics of hydrogens in double well potentials: The transition of the jump rate from the low temperature quantum-mechanical to the high temperature activated regime, *J. Chem. Phys.* **95,** 4201–4214 (1991).
58. M. Neumann, D. F. Brougham, C. J. McGloin, M. R. Johnson, A. J. Horsewill, and H. P. Trommsdorf, Proton tunneling in benzoic acid crystals at intermediate temperatures: Nuclear magnetic resonance and neutron scattering studies, *J. Chem. Phys.* **109,** 7300–7311 (1998).
59. A. Kubo and C. A. Mc Dowell, One- and two-dimensional ^{31}P cross-polarization magic-angle spinning nuclear magnetic resonance studies on two-spin systems with homonuclear dipolar coupling and J coupling, *J. Chem. Phys.* **92,** 7156–7170 (1990).
60. R. Tycko and S. O. Smith, Symmetry principles in the design of pulse sequences for structural measurements in magic angle spinning nuclear magnetic resonance, *J. Chem. Phys.* **98,** 932–943 (1993).
61. I. Schnell, Doppelquantenspektroskopie an polykristallinen Phosphaten, Diploma thesis, Johannes Gutenberg University, Mainz, Germany (1996).
62. J. Schmedt auf der Günne and H. Eckert, High-resolution double-quantum ^{31}P NMR: A new approach to structural studies of thiophosphates, *Chem. Eur. J.* **4,** 1762–1767 (1998).
63. K. T. Mueller, Analytic solutions for the time evolution of dipolar-dephasing NMR signals, *J. Magn. Reson. A* **113,** 81–93 (1995).
64. T. Gullion, D. B. Baker, and M. S. Conradi, New compensated Carr–Purcell sequences, *J. Magn. Reson.* **89,** 479–484 (1990).